

Postprint: Carbide Evolution Behavior in High-Tungsten K416B Cast Nickel-Based Alloy During High-Temperature Creep

Authors: Xie Jun, Yu Jinjiang, Sun Xiaofeng, Jin Tao, Sun Yuan

Date: 2023-03-19T00:00:00+00:00

Abstract

The evolution behavior of precipitates during high-temperature creep of high-tungsten K416B nickel-based superalloy was investigated through creep performance testing and microstructural morphology observation. The results indicate that in the as-cast alloy, the γ' phase exhibits non-uniform size distribution and strip-like MC carbides are distributed in a Chinese-character pattern within interdendritic regions; during high-temperature creep under applied stress, fine M₆C carbides can precipitate discontinuously in the deformed matrix, and thermodynamic analysis suggests that under stress-induced effects, carbon element segregates at stress concentration sites and combines with carbide-forming elements such as tungsten, thereby promoting the precipitation of fine M₆C phase from the matrix; simultaneously, grooves form on the surfaces of strip-like MC carbides, which gradually decompose and transform into granular M₆C phase, wherein the additional stress formed on the surfaces of strip-like MC phase is the primary cause for the continuous dissolution and spheroidization of MC phase.

Full Text

ACTA METALLURGICA SINICA, Vol. 51, No. 4, April 2015, pp. 458-464

CARBIDE EVOLUTION BEHAVIOR OF K416B AS-CAST Ni-BASED SUPERALLOY WITH HIGH W CONTENT DURING HIGH TEMPERATURE CREEP

XIE Jun, YU Jinjiang, SUN Xiaofeng, JIN Tao, SUN Yuan
Institute of Metal Research, Chinese Academy of Sciences, Shenyang 110016

Correspondent: YU Jinjiang, professor, Tel: (024)23971713, E-mail: jjyu@imr.ac.cn

Supported by National Basic Research Program of China (Nos.2010CB631200 and 2010CB631206) and National Natural Science Foundation of China (No.50931004)

Manuscript received 2014-10-08, in revised form 2014-12-22

ABSTRACT

As-cast Ni-based superalloys with high tungsten content are extensively used in aero-engine turbine vanes due to their excellent oxidation resistance and temperature capability. During high-temperature service, these materials undergo creep deformation and microstructural evolution, with creep behavior primarily governed by chemical composition and microstructural features such as the size, distribution, and morphology of γ' phase and carbides. Carbide morphology is particularly critical to creep resistance—dispersively distributed carbide particles generally enhance creep resistance, whereas continuously distributed carbides along boundaries provide easy paths for crack propagation and degrade mechanical properties. Furthermore, creep life depends significantly on microstructural evolution at elevated temperatures. However, the carbide evolution mechanism in K416B superalloy during creep remains unclear.

This study investigates the evolution behavior of precipitates in K416B Ni-based superalloy with high W content during high-temperature creep through creep property testing and microstructural observation. The results show that the γ' phase exhibits inhomogeneous size in the as-cast alloy, with stripe-like MC carbides distributed in Chinese-script morphology in interdendritic regions. During high-temperature creep under applied stress, fine M₆C carbides discontinuously precipitate in the deformed γ matrix. Thermodynamic analysis indicates that carbon segregates at stress concentration sites and combines with carbide-forming elements such as W, promoting precipitation of fine M₆C from the γ matrix. Simultaneously, grooves form on the surfaces of stripe-like MC carbides, which gradually decompose and transform into granular M₆C particles. The additional stress generated on MC carbide surfaces is identified as the primary factor driving continuous dissolution and spheroidization of MC phase.

KEY WORDS K416B Ni-based superalloy, creep, carbide evolution, thermodynamics analysis

1. Introduction

High-tungsten cast nickel-based superalloys are considered important materials for manufacturing aero-engine turbine guide vanes due to their excellent oxidation resistance and temperature capability [1-3]. K416B nickel-based superalloy contains up to 16.3 wt% W and exhibits good thermal fatigue performance, making it one of the equiaxed cast superalloys with higher temperature-bearing

capacity [4]. Tungsten is a crucial solid-solution element in nickel-based superalloys, with a partition ratio of approximately 1:1 between γ and γ' phases, simultaneously strengthening both phases and improving creep resistance [5-7]. Additionally, W is a primary carbide-forming element that forms various types and morphologies of carbides during solidification [8,9], directly affecting mechanical properties. Studies on high-tungsten M963 alloy [10,11] have shown that as melt processing temperature increases, carbide morphology transforms from blocky to granular with more uniform distribution, thereby improving stress rupture properties. During high-temperature thermal exposure, carbides in Ni-Cr-W alloys can undergo decomposition reactions ($M6C \rightarrow M23C6 + M$ (W, Ni, Cr, Mo)), with M23C6 carbides precipitating along grain boundaries and maintaining specific orientation relationships with the matrix: (100)M23C6 // (100)matrix [12,13]. Furthermore, research [14-16] indicates that after long-term aging, carbides in cast nickel-based alloys can transform as $MC + \gamma \rightarrow + M23C6$ (M6C), with the amount of secondary M23C6 (M6C) carbides increasing with higher aging temperatures and longer durations.

During high-temperature service, nickel-based superalloys undergo microstructural evolution including γ' phase coarsening and rafting, carbide transformation (such as $MC \rightarrow M23C6$ or M6C), and secondary precipitation of strengthening phases (γ' and carbides) [17,18]. This evolution is closely related to service life [19]. The microstructure of high-tungsten K416B alloy consists primarily of γ phase, γ' phase, and carbides. During high-temperature creep, creep deformation inevitably occurs accompanied by precipitate transformation, yet the carbide evolution mechanism in high-tungsten alloys during creep remains unclear.

This work investigates the evolution mechanism of precipitates in K416B alloy during high-temperature creep through creep testing and microstructural observation using scanning electron microscopy (SEM) and transmission electron microscopy (TEM), aiming to provide theoretical basis for alloy development and application.

2. Experimental Methods

K416B master alloy ingots were remelted in a 10 kg vacuum induction furnace and cast into equiaxed crystal bars. The nominal composition (wt.%) was: C 0.13, Cr 4.90, Co 6.82, Nb 2.06, Al 5.75, W 16.3, Ti 1.00, Hf 1.00, Ni balance. The alloy bars were machined into cylindrical creep specimens with a gauge length of 25 mm and diameter of 5 mm. Creep tests were conducted at 1000 °C under 150 MPa stress for various durations using an F-25 creep/stress rupture testing machine.

Creep-interrupted specimens were ground and polished, then chemically etched using a solution of 20 mL HCl + 5 g CuSO₄ + 25 mL H₂O. Microstructural observation and energy-dispersive spectroscopy (EDS) analysis of precipitates

were performed using an S-3400N SEM. For TEM analysis, 0.5 mm thick slices were cut from creep-interrupted specimens, mechanically thinned to 50 μm on both sides, and punched into 3 mm diameter discs. TEM samples were prepared by twin-jet electropolishing at $-25\text{ }^{\circ}\text{C}$ using a 10% perchloric acid ethanol solution. A TECNAI-20 TEM was used to examine the microstructure of creep-to-fracture specimens.

3. Experimental Results

3.1 Creep Behavior and Microstructural Evolution

The creep curve of K416B alloy at $1000\text{ }^{\circ}\text{C}$ under 150 MPa is shown in [Figure 1: see original paper]. The alloy exhibits a low steady-state creep rate of approximately $0.00716\text{ }\%/h$ with a steady-state duration of about 120 h, achieving a creep life of 154 h and post-fracture elongation of 4.7%.

The microstructure of as-cast K416B alloy is presented in [Figure 2: see original paper]. The γ' phase shows inhomogeneous size distribution, with larger γ' particles (1-2 μm) irregularly distributed in interdendritic regions [FIGURE:2a, upper right], while smaller γ' particles (0.3-0.6 μm) are observed in dendrite cores [FIGURE:2a, lower left]. [Figure 2b: see original paper] shows carbide precipitation morphology in the as-cast alloy, revealing stripe-like MC carbides with straight surfaces distributed in Chinese-script patterns in interdendritic regions.

Microstructures after different creep durations at $1000\text{ }^{\circ}\text{C}$ under 150 MPa are shown in [Figure 3: see original paper], where 5 h, 50 h, and 154 h correspond to primary, steady-state, and tertiary creep stages, respectively. After 5 h of creep, slight coarsening of interdendritic γ' phase occurs with minimal deformation and only a few white particles precipitated [Figure 3a: see original paper]. After 50 h, significant γ' coarsening and rafted structure formation are observed, accompanied by increased precipitation of fine white particles [Figure 3b: see original paper]. In the creep-to-fracture condition [Figure 3c: see original paper], the rafted γ' structure becomes distorted and irregularly distributed, with further increased fine white particles. EDS analysis reveals these particles are rich in W, Cr, and C, indicating that numerous fine particles precipitate dispersively in the deformed matrix during creep compared to the as-cast condition [Figure 2a: see original paper].

The evolution of stripe-like carbides in interdendritic regions during creep at $1000\text{ }^{\circ}\text{C}$ under 150 MPa is shown in [Figure 4: see original paper]. After 5 h, grooves form on carbide surfaces, creating an uneven morphology [Figure 4a: see original paper]. After 50 h, groove depth increases and local regions of stripe carbides undergo fission into granular particles [Figure 4b: see original paper]. At fracture, stripe carbides are completely fissioned into granular particles distributed discontinuously [Figure 4c: see original paper], demonstrating that

stripe-like carbides gradually fuse into discontinuous granular particles during high-temperature creep.

TEM images of stripe-like carbides during creep at 1000 °C under 150 MPa are presented in [Figure 5: see original paper]. After 50 h, stripe carbides show uneven surfaces with a few slip dislocations terminating at the carbides, indicating effective obstruction of dislocation motion. EDS analysis shows these stripe precipitates are rich in Nb, W, Hf, Ti, and C, and the corresponding selected-area electron diffraction (SAED) pattern [inset in [Figure 5: see original paper]a] identifies them as MC-type carbides.

[Figure 5: see original paper]b shows TEM images of fissioned carbides in the crept-to-fracture specimen. Noticeable dissolution grooves form on carbide surfaces with numerous dislocation traces nearby. The fissioned granular particles are rich in W, Nb, Cr, and C, and SAED analysis [inset in [Figure 5: see original paper]b] identifies them as M6C-type carbides. This indicates that interdendritic stripe-like MC carbides transform into granular M6C carbides during high-temperature creep.

[Figure 6: see original paper] shows the microstructure of K416B alloy crept to fracture at 1000 °C under 150 MPa for 154 h. Fine granular carbides precipitate dispersively at dislocation pile-up sites and γ/γ' interfaces. SAED analysis [inset in [Figure 6: see original paper]a] identifies these as M6C carbides, with numerous deformation dislocations tangled around them. In another region, fissioned carbides show chain-like distribution with mobile dislocations piled up at granular carbides, demonstrating that both secondary fine carbides and fissioned granular carbides effectively hinder dislocation motion and improve creep resistance.

4. Discussion

4.1 Stress-Induced Precipitation of Fine Carbides

During steady-state creep at 1000 °C under 150 MPa, K416B superalloy exhibits a low creep rate of 0.00716 %/h. As creep progresses, the γ matrix deforms more than the stronger γ' phase, leading to increased dislocation density and stress concentration in the matrix and at interfaces, creating high flow stress. This provides favorable conditions for fine carbide precipitation in the matrix, promoting dispersive precipitation of M6C from the deformed alloy [Figure 6a: see original paper], indicating that stress induction enables fine carbide precipitation during creep.

Stress-induced precipitation can be analyzed using phase equilibrium thermodynamics. The high W content (16.3%) in as-cast K416B alloy and absence of fine carbides in the as-cast matrix [Figure 2a: see original paper] indicate that carbon is in equilibrium, providing necessary conditions for M6C precipitation. During creep, plastic deformation of the matrix increases the chemical potential

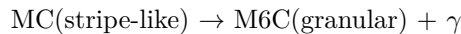
of carbon in the γ phase, creating supersaturation. Additionally, crystal slip and plastic deformation release deformation heat, promoting precipitation of fine M6C in the γ matrix. The effect of applied stress on carbon solubility can be analyzed using thermodynamic theory of stress effects on phase equilibrium [20]. The relationship is given by:

$$X_C^\sigma = X_C^0 \exp\left(-\frac{\sigma V}{RT}\right)$$

where X_C^σ and X_C^0 are the mole fractions of solute C dissolved in the γ phase with and without applied stress, respectively; σ is the applied stress; R is the gas constant; T is thermodynamic temperature; and V is the molar volume. This equation shows that applied stress affects carbon solubility in the γ phase. During creep under tensile stress, σ is negative, making the exponential term < 1 , indicating that tensile stress reduces carbon solubility in the γ phase. During tensile creep, increasing dislocation density releases deformation heat while causing carbon segregation at stress concentration sites. With its small atomic radius and thermodynamic activity for carbide formation, carbon combines with strong carbide-forming elements like W and Cr, promoting discontinuous precipitation of carbides in the matrix or at γ/γ' interfaces.

4.2 Evolution Mechanism of Stripe-Like Carbides

EDS analysis shows that Nb, W, Hf, and Ti are the main constituents of stripe-like MC carbides, while fissioned M6C carbides are rich in W, Nb, and Cr. These carbide-forming elements are collectively designated as Y elements. Since both MC and M6C carbides have fcc structures, stripe-like MC carbides can transform into secondary M6C during stressed high-temperature creep [Figure 5: see original paper], with the transformation reaction expressed as:



The fission process can be analyzed using equilibrium thermodynamics. During creep, stripe-like carbides effectively obstruct dislocation motion [Figure 5: see original paper], creating stress concentration and generating additional stress $P_{MC/\gamma}$ at their surfaces. Combining with the previous equation yields:

$$X_Y^\gamma = X_Y^{MC} \exp\left(-\frac{P_{MC/\gamma} V_{MC}}{RT}\right)$$

where X_Y^{MC} and X_Y^γ are the mole concentrations of Y element in MC and γ phases, respectively, and V_{MC} is the molar volume of MC carbide. As creep progresses and matrix deformation increases, the additional stress on stripe-like MC surfaces increases, raising the concentration of Y element in adjacent γ phase and accelerating diffusion of Y from MC to γ matrix, thus promoting MC decomposition.

The additional stress ($P_{MC/\gamma}$) generated by applied stress at the MC/ γ interface significantly affects the equilibrium concentration of Y element, causing groove formation and eventual spheroidization of stripe-like MC carbides. This process is illustrated in [Figure 7: see original paper]. In as-cast K416B alloy, stripe-like MC surfaces are smooth. During stressed creep, $P_{MC/\gamma}$ develops at the MC/ γ interface [Figure 7a: see original paper], leading to groove formation under stress [Figure 7b: see original paper]. The instantaneous balance between interface tension and $P_{MC/\gamma}$ at groove intersections is:

$$\sigma_{MC/\gamma} \cos \alpha = P_{MC/\gamma}$$

where $\sigma_{MC/\gamma}$ is the interface tension between MC phase and γ matrix at the groove, and α is the groove angle. As creep continues, Y elements continuously diffuse from MC to adjacent γ phase under additional stress, creating high-concentration regions that subsequently diffuse toward low-concentration areas, with Y also diffusing from γ into stripe-like MC, gradually transforming it into granular M6C [Figure 7c: see original paper]. This disrupts interface tension balance at groove intersections. To maintain equilibrium, the curved front of granular M6C continuously dissolves, with the interface tension relationship during spheroidization being:

$$\sigma_{MC/\gamma} \cos \alpha' = P_{MC/\gamma}$$

Thus, the additional stress $P_{MC/\gamma}$ on stripe-like MC surfaces is the primary factor driving groove deepening and MC decomposition. In other words, under combined strain and interface energy, elemental diffusion deepens grooves and increases thickness, causing adjacent MC phases to decompose into granular M6C.

4.3 Effect of Microstructural Evolution on Creep Performance

During stressed high-temperature creep, fine M6C carbides precipitate discontinuously at dislocation pile-up sites and γ/γ' interfaces through stress induction. As creep progresses, the number of fine M6C precipitates increases [Figure 3: see original paper], effectively hindering dislocation motion [Figure 6a: see original paper]. The strengthening effect [23] can be expressed as:

$$\Delta\sigma = \frac{k\eta f^{1/2}}{r}$$

where $\Delta\sigma$ is the strengthening effect from fine carbides, r is the average radius of fine carbide particles, f is the volume fraction of precipitated fine carbides, and η and k are material constants. This shows that increasing fine M6C precipitation (increasing f) enhances creep resistance, contributing to the alloy's low steady-state creep rate.

Previous studies [24,25] indicate that during creep, deformation dislocations easily pile up at stripe-like phases, creating stress concentration. When this concentrated stress exceeds the bonding strength between the stripe-like phase and matrix, cracks initiate and propagate along the interface, accelerating fracture and creating weak links. In contrast, granular phase regions are less prone to stress concentration and provide dispersion strengthening, improving alloy strength [26]. Therefore, transformation of stripe-like MC carbides into granular M₆C during creep helps relieve stress concentration, improves creep strength, and extends the steady-state duration of K416B alloy.

5. Conclusions

1. In as-cast K416B alloy, the γ' phase shows inhomogeneous size and irregular distribution in both interdendritic and dendrite core regions, with stripe-like MC carbides distributed in Chinese-script patterns in interdendritic regions.
2. During high-temperature creep, fine granular M₆C carbides precipitate dispersively through stress induction. Applied stress reduces carbon solubility in the γ matrix, causing carbon segregation at stress concentration sites where it combines with carbide-forming elements like W, promoting discontinuous precipitation of fine M₆C in the matrix and at γ/γ' interfaces.
3. During stressed high-temperature creep, stripe-like MC carbides become coarsened and uneven, gradually dissolving and transforming into granular M₆C. The additional stress formed on MC carbide surfaces is the primary factor driving continuous decomposition and spheroidization of MC phase.

References

- [1] Liu Y, Hu R, Li J S, Kou H C, Li H W, Chang H, Fu H Z. *Mater Sci Eng*, 2009; A508: 141
- [2] Kim I S, Choi B G, Hong H U, Do J, Jo C Y. *Mater Sci Eng*, 2014; A593: 55
- [3] Zhang G Q. *Acta Metall Sin (Engl Lett)*, 2005; 18: 55
- [4] Yang Y H, Yu J J, Sun X F, Jin T, Guan H R, Hu Z Q. *Mater Des*, 2012; 36: 699
- [5] Tang B, Jiang L, Hu R, Li Q. *Mater Charact*, 2013; 78: 144
- [6] Zhen Y R, Xie J Z. *J Aeronaut Mater*, 2009; 29(6): 1
- [7] Qin X Z, Guo J T, Yuan C, Hou J S, Ye H Q. *Mater Lett*, 2008; 62: 185
- [8] Hou J S, Guo J T, Wu Y X, Zhou L Z, Ye H Q. *Mater Sci Eng*, 2010; A527: 1548
- [9] Zheng L, Gu C Q, Zeng Q, Hou S E. *J Aeronaut Mater*, 2004; 24(1): 17

- [10] He L Z, Sun X F, Zheng Q, Hou G C, Zhang C Z, Guan H R, Hu Z Q. Mater Eng, 2004; (2): 40
- [11] Yuan C, Sun X F, Yin F S, Guan H R, Hu Z Q, Zheng Q, Yu Y. J Mater Sci Technol, 2001; 17: 425
- [12] Bai G H, Li J S, Hu R, Zhang T B, Kou H C, Fu H Z. Mater Sci Eng, 2011; A528: 2339
- [13] Yang J X, Zheng Q, Sun X F, Guan H R, Hu Z Q. Mater Sci Eng, 2007; A465: 100
- [14] Qin X Z, Guo J T, Yuan C, Hou J S, Ye H Q. Mater Sci Forum, 2007; 546-549: 1301
- [15] Yang J X, Sun Y, Jin T, Sun X F, Hu Z Q. Acta Metall Sin, 2014; 50: 839
- [16] Xiao X, Zeng C, Hou J S, Qin X Z, Guo J T, Zhou L Z. Acta Metall Sin, 2014; 50: 1031
- [17] Wang L, Wang S, Song X, Liu Y, Xu G H. Int J Fatigue, 2014; 62: 2
- [18] Yang J X, Zheng Q, Sun X F, Guan H R, Hu Z Q. Mater Sci Eng, 2006; A429: 341
- [19] Seo S M, Kim I S, Lee J H, Jo C Y, Miyahara H, Ogi K. J Met Sci Technol, 2008; 24: 110
- [20] Mats H, translated by Lai H Y, Liu G X. Alloy Diffusion and Thermodynamic. Beijing: Metallurgical Industry Press, 1984: 103
- [21] Mats H, translated by Li Q B, Wang X C. Diffusion Controlled Reactions in Alloy and Thermodynamic of Alloy. Shenyang: Liaoning Science and Technology Press, 1984: 204
- [22] Lvov G, Levit V I, Kaufman M J. Metall Mater Trans, 2004; 35A: 1675
- [23] Mao W M, Zhu J C, Li J, Long Y, Fan Q C. The Structure and Properties of Metallic Materials. Beijing: Tsinghua University Press, 2008: 186
- [24] Tian S G, Wang M G, Li T, Qian B J, Xie J. Mater Sci Eng, 2010; A527: 5444
- [25] Xie J, Tian S G, Zhou X M, Yu X F, Wang W X. Mater Sci Eng, 2012; A538: 306
- [26] He L Z, Zheng Q, Sun X F, Guan H R, Hu Z Q, Tieu A K, Lu C, Zhu H T. Metall Mater Trans, 2005; 36A: 2385

Note: Figure translations are in progress. See original paper for figures.

Source: ChinaXiv – Machine translation. Verify with original.